

The statistics of the points where nodal lines intersect a reference curve

Amit Aronovitch and Uzy Smilansky

Department of Physics of Complex Systems, The Weizmann Institute of Science, 76100 Rehovot, Israel

E-mail: amit.aronovitch@weizmann.ac.il

Received 25 April 2007, in final form 25 June 2007

Published 24 July 2007

Online at stacks.iop.org/JPhysA/40/9743

Abstract

We study the intersection points of a fixed planar curve Γ with the nodal set of a translationally invariant and isotropic Gaussian random field $\Psi(\mathbf{r})$ and the zeros of its normal derivative across the curve. The intersection points form a discrete random process which is the object of this study. The field probability distribution function is completely specified by the correlation $G(|\mathbf{r} - \mathbf{r}'|) = \langle \Psi(\mathbf{r})\Psi(\mathbf{r}') \rangle$. Given an arbitrary $G(|\mathbf{r} - \mathbf{r}'|)$, we compute the two-point correlation function of the point process on the line, and derive other statistical measures (repulsion, rigidity) which characterize the short- and long-range correlations of the intersection points. We use these statistical measures to quantitatively characterize the complex patterns displayed by various kinds of nodal networks. We apply these statistics in particular to nodal patterns of random waves and of eigenfunctions of chaotic billiards. Of special interest is the observation that for monochromatic random waves, the number variance of the intersections with long straight segments grows like $L \ln L$, as opposed to the linear growth predicted by the percolation model, which was successfully used to predict other long-range nodal properties of that field.

PACS numbers: 05.45.Mt, 05.40.-a, 03.65.Sq

(Some figures in this article are in colour only in the electronic version)

1. Introduction

Entangled planar networks of convoluted lines appear quite often in various studies in physics and mathematics. To cite a few examples, recall the snapshots of polymer solutions, the level sets of rugged terrain, the trajectories of Brownian particles [1], the domain boundaries in magnetic materials or in simulations of random percolation [2] etc. To characterize such networks in a concise and quantitative way, one usually recurses to statistical measures,

chosen to describe the specific properties of the network which are relevant to the problem at hand. Some studies give bounds on the length or the curvature of the nodal lines of wavefunctions in bounded domains, in other instances, the distribution of fractal dimensions of Brownian trajectories which provide an impression of their ruggedness [3]. Other examples are the distribution of the areas of connected domains in critical percolation, which show a universal power law, or the (properly normalized) number of bulk nodal domains in billiard wavefunctions which follow universal patterns that distinguish between chaotic and integrable billiards [4, 5]. None of these measures provide a complete description of the complexity of the network under study, and there is always room for introducing new measures which shed light on features which were not brought to the front by previous studies.

In the present work we are interested in the point process generated by the intersections of a complex network of lines with a given reference curve. To the best of our knowledge, previous studies of the statistics of such point processes were not as detailed as the corresponding analysis for other systems (such as energy spectra, eigenvalues of random matrices, or one-dimensional gas). In particular, while the density and correlation function were calculated, other physically meaningful observables which can be extracted from them, such as the number variance, rigidity and the correlation form factor (power spectrum) were not investigated.

Longuet-Higgins, in his analysis of the moving surface of the sea [6], derived the density and correlation functions of the zeros on a straight line. Berry and Dennis [7] studied the distribution of phase singularities in a random complex field. For a planar field, these singularities are actually the intersections of the nodal lines of the real part of the field with those of the imaginary part. In these cases (and others as well, including the present paper), restricting the field to a straight line allows using the formula derived by Rice [8] for calculating the exact correlation of the zeros from the known two-point correlation of the amplitudes. Blum *et al* [4] considered billiard wavefunctions, and studied the number of intersections of their nodal lines with the billiard boundary. It was shown that the distributions of the (properly normalized) number of intersections distinguish between chaotic and integrable billiards. Johansson [1] considered the trajectories of N Brownian particles on a line, which start equally separated at $t = 0$ and return to their original position at $t = 2T$ without intersecting each other's path. The distribution of spacings at $t = T$, measured in units of the average spacing, was shown to be identical to the distribution of eigenvalues in the Gaussian unitary ensembles of $N \times N$ matrices (GUE). Baik and Rains [9] showed that for a certain class of discrete, non-intersecting random walkers, when not restricted to return to the original position, the limiting distribution of spacings matches that of the eigenvalues of the Gaussian orthogonal ensemble (GOE). Such problems, when considered in (x, t) space, represent intersections of random planar paths with a reference line orthogonal to the t axis.

In the present paper we shall study the points generated by the intersection of a reference curve with the nodal lines of three fields.

- (i) Random monochromatic waves [10] in \mathbb{R}^2 which are solutions of the wave equation

$$-\Delta\Psi(x, y) = k^2\Psi(x, y). \quad (1)$$

Since no boundary conditions are required, the solutions are plane waves which propagate in arbitrary directions with wave vectors $|\mathbf{k}| = k$. The random wave ensemble can be constructed as a linear superpositions of plane waves

$$\sqrt{\frac{2}{N}} \sum_{n=1}^N \cos(\mathbf{k}_n \mathbf{r} + \phi_n), \quad (2)$$

(with $\mathbf{r} \in \mathbb{R}^2$, $|\mathbf{k}_n| = k$ and $N \gg 1$), where $\mathbf{k}_n/|k|$ and ϕ_n are distributed uniformly and independently on the unit circle. Equivalently, one can also use random superpositions of solutions of the wave equation (1) in polar coordinates

$$a_0 J_0(kr) + 2 \sum_{l>0} a_l J_l(kr) \cos(l\theta + \phi_l), \tag{3}$$

with real coefficients a_l , which are identically and independently distributed Gaussian variables, and where the phases ϕ_l are independent and uniformly distributed on $[0, 2\pi]$. The correlation function for this Gaussian ensemble is

$$G_{\text{RW}}(\mathbf{r}, \mathbf{r}') = J_0(k|\mathbf{r} - \mathbf{r}'|). \tag{4}$$

- (ii) Given a reference curve, we consider the normal derivative $\mathbf{n} \cdot \nabla \psi(\mathbf{r})$ of the random wave field (2), where \mathbf{n} is the direction normal to the reference curve at \mathbf{r} . For example, when the curve is the x axis, the two-point correlation of this function is

$$G_{\text{NRW}}(x, x') = 2J_1(k|x - x'|)/(k|x - x'|) \tag{5}$$

The zeros of the normal derivative are not, strictly speaking, nodal intersections, but they do define a point process, which can be studied the same way. Furthermore, when the reference curve is straight, these zeros are the nodal intersections of an actual random field.

The boundary modified random waves [11] were introduced in order to study the effect of a Dirichlet boundary on the statistics of the nodal set. They are defined in the upper-half plane and are solutions of (1) subject to the boundary condition

$$\Psi(x, y = 0) = 0 \tag{6}$$

As explained in section 4, the nodal intersections of that field with its boundary, the x axis, are identical with the zeros of the normal derivative of a Gaussian random wave field on this line. This fact makes the normally derived random wave field on a curved line a natural candidate for comparison with generalized boundary modified models, such as Wheeler’s generalization for a circular boundary [12], or the semi-classical treatment of a general boundary by Urbina and Richter [13].

- (iii) Random Gaussian fields with the short-range correlation function

$$G_{\text{SRF}}(\mathbf{r}, \mathbf{r}') = \exp(-k^2|\mathbf{r} - \mathbf{r}'|^2/4) \tag{7}$$

were introduced in [14] to investigate the importance of the fact that the random waves correlation function decays very slowly. The correlation function above coincides with G_{RW} at short ranges, but decays quickly at large values.

According to the Uhlenbeck theorem [15], the crossing probability of nodal lines of random waves vanishes. In [16], the ‘avoidance’ of nodal lines was defined, as a measure of the distance between nodal lines which avoid intersection in the vicinity of saddle points. The probability distribution $P(d)$ of the avoidances d was computed and it displayed linear repulsion at small values of d , $P(d) \propto d$. However, the coefficient of proportionality was not the same as one would get from the application of Johansson’s result to the case of Brownian trajectories.

Having in mind the results of Johansson’s paper on the one hand, and knowing that nodal lines avoidances repel linearly on the other hand, one might expect that the statistics of nodal intersections would also follow (at least to some extent) the predictions of random matrix theory. We shall show below that this is not the case.

This paper is constructed as follows. In section 2, we discuss the derivation of the nodal intersection statistics from the known distribution of the amplitudes. First, we extract

the necessary one-dimensional correlation functions which follow from restricting the field to a general reference curve (similar to the restriction of the amplitude to a straight line, which was done in [6]). Then, the statistics of the zeros is extracted from these one-dimensional amplitude correlations. An exact formula for computing zeros correlations from one-dimensional amplitude correlations was derived by Rice in his analysis of random noise [8, 17]. The derivation described here uses a different method, and is similar to the derivation used by other authors [7, 18]. However, as opposed to these studies, we consider the case of a general curve, and derive the formulae for the line and the circle as special cases. Restriction to a general curve does not preserve the field's translational invariance. This makes the results more complicated, but the methods remain the same. Such a generalization is necessary in cases where the test curve is inherent in the problem we wish to model (such as the boundary of a quantum billiard), and not independent of the field. In appendix B we describe the generalized calculation for the normally derived random waves.

In section 3, we apply the above to the monochromatic random wave (2), using a circle and a straight line for reference curves. A universal correlation function is extracted for the semiclassical ($k \gg 1$) limit, and found to decay slower than the RMT correlations. The number variance and the form factor (29) are calculated and their special features, which are clearly different from the RMT predictions, are shown as well. Over large ranges, the number variance is shown to grow as $L \ln L$. This is in contrast with the linear growth we might expect from Bogomolny's percolation model [5], whose predictions for other asymptotic properties of the field (nodal count [4] and SLE driving force [19]) give a satisfactory match to numerical data. In section 4, we discuss the zeros distribution of the normal derivative of a Gaussian field on the reference curve. In the framework described above this may be considered a different form of restricting the field to the curve. The semiclassical limit, number variance and form factor are calculated for this case too.

Finally, in section 5 we compare the above results to those of other fields. The statistics mentioned above are calculated for the short-range Gaussian model (7) (which displays a different behaviour), and also evaluated numerically for chaotic billiards, which show a reasonable match to the monochromatic random wave model. The theoretical properties of the distributions considered are summarized in table 1 (page 23), and compared to the well-known results for the Poisson process and RMT ensembles.

2. Statistics of zeros from amplitude correlations

2.1. Nearest neighbour distribution

When considering the statistics of a sequence of points, the nearest neighbour spacing distribution (where the spacing is measured in units of the mean spacing) is perhaps the most natural, and easy to evaluate experimentally. In figure 1, we show the nearest neighbour distributions for two-point processes. The first is the intersections of the nodal lines of the random wave (RW) field (2) with the reference curve. The second process (NRW) is the zeros of the normal derivative of the random waves on the curve. The distributions were generated by numerical simulations, and compared with the corresponding statistics of the random (Poisson) ensemble and the Wigner surmise (corresponding to the GOE ensemble) [20]. At short ranges, both ensembles display linear level repulsion similar to the GOE distribution, but with different slopes. The most conspicuous differences appear at large spacings, and to get a clearer impression, we show in figure 2, the same data in semi-log plot. We observe two important differences.

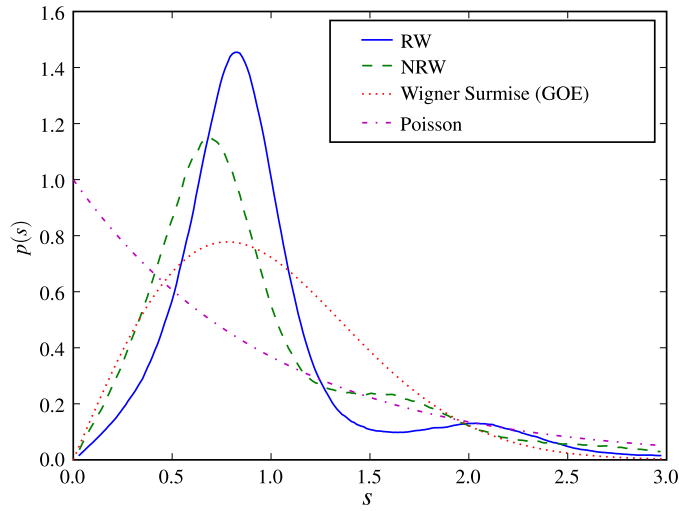


Figure 1. Density of the nearest neighbour level spacing.

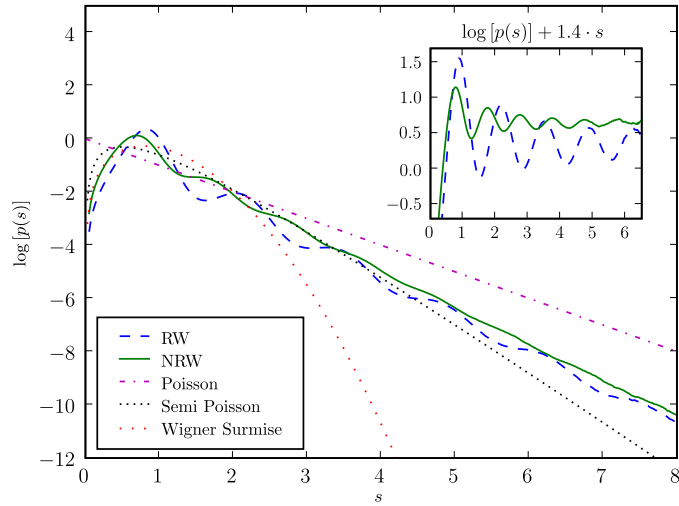


Figure 2. Nearest neighbour level spacing (log density). Inset shows persistent oscillations relative to the mean decaying curve.

- (i) On average, both distributions decay exponentially with approximately the same rate $p(s) \sim \exp(-1.4s)$. This decay is faster than the $\exp(-s)$ Poisson decay, but slower than the ‘semi-Poisson’ [21] distribution, which decays like $\exp(-2s)$.
- (ii) The overall exponential decays are decorated by persistent oscillations, which are clearly seen in the inset of figure 2. The oscillations have slowly decaying amplitudes and their frequencies are $\sim 1.4\pi$ for RW and $\sim 2\pi$ for NRW.

The results above demonstrate that the nodal intersection statistics are significantly different than those of other, well-known, point processes. The purpose of this work is to investigate the reasons for the occurrence of these differences. However, the nearest neighbour statistic is not easily amenable to analytic derivation. Rather, we use the two-point correlation function, which is readily accessible, as will be shown in this paper. For the asymptotic $s \ll 1$

limit, this statistic coincides with the nearest neighbour density. Furthermore, other statistics with well-defined physical meaning, such as the form factor and number variance, can be expressed in terms of the correlation. We will now give some definitions, and follow with an overview of a derivation for the two-point correlation of nodal intersections with a general reference curve.

2.2. Two-point correlations

A random field $\psi(\mathbf{r})$ is Gaussian if for any vector \mathbf{u} whose elements u_1, u_2, \dots, u_n are field amplitudes $u_i = \psi(\mathbf{r}_i)$ or partial derivatives of the field at some points $\mathbf{r}_1, \dots, \mathbf{r}_n$, the probability distribution of \mathbf{u} is multivariate normal. The probability density of a multivariate normal random vector \mathbf{u} , with a mean value \mathbf{u}_0 is given by

$$p(\mathbf{u}) = \frac{1}{(2\pi)^{n/2} \sqrt{\det C}} \exp \left[-\frac{1}{2} (\mathbf{u} - \mathbf{u}_0)^T C^{-1} (\mathbf{u} - \mathbf{u}_0) \right], \tag{8}$$

where C is the covariance matrix $C_{i,j} = \text{Cov}(u_i, u_j)$. For the random wave ensemble (2), Gaussianity follows from the n -dimensional central limit theorem.

Assuming smoothness of the field, means and covariances of the field's derivatives can be calculated by deriving the appropriate amplitude statistics. Combining that with the fact that all the elements of \mathbf{u}_0 and C are single-point means and two-point covariances, it follows that all statistical properties of a Gaussian field $\psi(\mathbf{r})$ are completely determined by its mean value $\langle \psi(\mathbf{r}) \rangle$ (which will be zero for the relevant cases investigated) and the two-point covariance function $G(\mathbf{r}, \mathbf{r}') \equiv \text{Cov}(\psi(\mathbf{r}), \psi(\mathbf{r}'))$. As a consequence, we should be able to extract the distribution of the zeros from this function, and, in particular, the correlation function of the nodal intersections can be derived from the correlation function of the one-dimensional restriction $f(t) \equiv \psi(\mathbf{r}(t))$ of the investigated field to the given reference curve $\Gamma : [0, L] \rightarrow \mathbb{R}^2 \equiv \mathbf{r}(t)$ (t is the natural curve parameter).

The density and correlations of nodal intersections (NI) can be calculated directly once $f(t)$ and its properties are known, in particular we shall use the two-point correlations of the restricted field f and its derivative along the curve $\dot{f}(t) \equiv df/dt$:

$$\begin{aligned} C_0(t, t') &\equiv \text{Cov}(f(t), f(t')) & C_1(t, t') &\equiv \text{Cov}(f(t), \dot{f}(t')), \\ \tilde{C}_1(t, t') &\equiv \text{Cov}(\dot{f}(t), f(t')) & C_2(t, t') &\equiv \text{Cov}(\dot{f}(t), \dot{f}(t')). \end{aligned} \tag{9}$$

We will also use a lowercase c to denote the single-point limit of these, i.e. $c_0(t) \equiv C_0(t, t) = \text{Var}(f(t))$ etc.

2.3. Restricting the field to a curve

Before we write down expressions for C_0, C_1 and C_2 , let us take note of special properties of these functions, which follow from the symmetry of our field. The fields considered are translationally invariant. This implies that the mean and the variance of the field are constant over the domain. It allows us to apply a constant linear transformation $\psi = A\tilde{\psi} + B$, normalizing the field so that $\langle \psi(\mathbf{r}) \rangle = 0$ and $c_0 = \langle \psi^2(\mathbf{r}) \rangle = 1$ for all \mathbf{r} (this is true for equations (2) and (3); however, we will keep c_0 in our expressions below, to make explicit the effect of the multiplicative scaling).

Furthermore, assuming smoothness of ψ , it follows that

$$2\langle \psi(\mathbf{r}) \nabla \psi(\mathbf{r}) \rangle = \nabla \langle \psi^2(\mathbf{r}) \rangle = 0. \tag{10}$$

In general, the restricted fields are not translationally invariant. Therefore the computation of their correlations requires special attention, and will involve the geometric properties of the

reference curve, such as its curvature. However, in the limit $t \rightarrow t'$, one can still project (10) onto the curve, and conclude that $\tilde{C}_1(t, t') \rightarrow -C_1(t, t')$, and in particular $c_1 = 0$.

The fields we consider here are also isotropic¹, so the correlation function has the form $\langle \psi(\mathbf{r})\psi(\mathbf{r}') \rangle = G(|\mathbf{r} - \mathbf{r}'|)$. To make use of this property, we change the coordinates

$$\mathbf{u} = \mathbf{r} + \mathbf{r}', \quad \mathbf{d} = \mathbf{r} - \mathbf{r}',$$

so that derivatives with respect to \mathbf{u} vanish. Derivatives with respect to \mathbf{d} can be expressed in terms of the single-parameter function $G(d)$ (where $d = |\mathbf{d}|$).

This results in the following expressions for the correlation functions (9):

$$\begin{aligned} C_0 &= G(d) \\ C_1 &= -\dot{\mathbf{r}}' \cdot \hat{\mathbf{d}}G'(d), \quad \tilde{C}_1 = \dot{\mathbf{r}} \cdot \hat{\mathbf{d}}G'(d) \\ C_2 &= -\sum_{i,j} \dot{r}_i \left[\left(G'' - \frac{G'}{d} \right) \frac{d_i d_j}{d^2} + \frac{G'}{d} \delta_{i,j} \right] \dot{r}'_j, \end{aligned} \tag{11}$$

where $\mathbf{r}' \equiv \mathbf{r}(t')$, and $\hat{\mathbf{d}} \equiv \mathbf{d}/d$.

2.4. The nodal intersections statistics

The density of zeros of f takes the form

$$\rho(t) = \sum_i \delta(t - t_i) = \delta(f(t))|\dot{f}(t)|, \quad \text{where } f(t_i) = 0. \tag{12}$$

Following Kac [22], we use the Fourier representation

$$\langle \rho(t) \rangle = \frac{1}{2\pi^2} \int \int_{-\infty}^{\infty} \frac{d\xi d\eta}{\eta^2} \langle e^{i\xi f(t)} (1 - e^{i\eta f(t)}) \rangle.$$

This integral can be solved using elementary properties of multinormal variables (8). For any multinormal variable \mathbf{x} with zero mean, and real vector \mathbf{k} , the following identity holds:

$$\langle e^{i\mathbf{k} \cdot \mathbf{x}} \rangle = \exp \left(-\frac{1}{2} \sum_{i,j} k_i C_{i,j} k_j \right), \quad \text{where } C_{i,j} = \text{Cov}(x_i, x_j) \tag{13}$$

Using the Gaussianity of the field f , this identity can be applied to the mean density. The resulting integral separates into simple Gaussian integrals, and we get the following result for the density:

$$\langle \rho \rangle = \frac{1}{\pi} \sqrt{\frac{c_2}{c_0}}. \tag{14}$$

We now move on to two-point statistics. When dealing with ‘point processes’ (such as the zeros of f), whose amplitude is a sum of delta functions, $\langle \rho\rho' \rangle$ normally contains a delta function at $t = t'$, corresponding to the strong autocorrelation. It is customary to subtract this term, to regularize the correlation function at $t = t'$. Thus, the two-point correlation function is defined (e.g. in [20]) as

$$\begin{aligned} R(t, t') &= \left\langle \sum_{i \neq j} \delta(t - t_i) \delta(t' - t_j) \right\rangle \\ &= \langle \rho(t)\rho(t') \rangle - \delta(t - t')\langle \rho(t) \rangle. \end{aligned}$$

¹ An example of a random field which is *not* isotropic is the non-monochromatic random wave models used in [6], which have a finite average wavenumber vector (carrier wave).

Using the same approach as above, we write

$$\langle \rho \rho' \rangle = \left\langle \frac{1}{4\pi^4} \int \frac{d\xi d\eta d\xi' d\eta'}{\eta^2 \eta'^2} e^{i\xi f} (1 - e^{i\eta \dot{f}}) e^{i\xi' f'} (1 - e^{i\eta' \dot{f}'}) \right\rangle. \tag{15}$$

To make use of (13), we write down the covariance matrix of the four variables $(f, f', \dot{f}, \dot{f}')$ appearing in this expression (see definitions in (9)):

$$M = \begin{pmatrix} c_0 & C_0 & 0 & C_1 \\ C_0 & c_0 & \tilde{C}_1 & 0 \\ 0 & \tilde{C}_1 & c_2 & C_2 \\ C_1 & 0 & C_2 & c_2 \end{pmatrix} \equiv \begin{pmatrix} A & C \\ C^T & B \end{pmatrix} \tag{16}$$

(A, B, C stand for the 2×2 submatrices).

Applying (13) to (15) we get more complicated integrals, which are nevertheless solvable (derivation in appendix A). The resulting expression for $R(t, t')$ is

$$R(t, t') = \frac{1}{\pi^2} \frac{a}{|A|^{3/2}} (\sqrt{1 - \hat{c}^2} + \hat{c} \arcsin(\hat{c})),$$

where $a = c_2|A| - c_0|C|$, $\hat{c} = (C_2|A| - C_0|C|)/a$, $|A| = c_0^2 - C_0^2$ and $|C| = -C_1\tilde{C}_1$ (here $|A|$ and $|C|$ stand for determinants—not absolute value).

From this, the normalized correlation coefficient $\mathcal{R} \equiv R/\langle \rho \rangle^2 - 1$, from which we will derive the other two-point statistics, follows immediately:

$$\mathcal{R}(t, t') = \frac{c_0}{c_2} \frac{a}{|A|^{3/2}} (\sqrt{1 - \hat{c}^2} + \hat{c} \arcsin(\hat{c})) - 1. \tag{17}$$

3. Simple curves in monochromatic random fields

The monochromatic Gaussian field (2) is often used as a statistical model for eigenfunctions of chaotic billiards. In this context, the ‘semiclassical’ regime (large k) has special significance. In terms of our statistical system, this means that we would be particularly interested in the $k \gg \kappa$ limit (where κ is the curvature of the reference curve). In this regime, the first approximation for the curve is a straight line, and the second one is a circular arc. These two cases are also important for their simplicity—in both cases, the domain distance d between two points on the curve depends only on the curve distance $|t - t'|$, so (11) assumes a simpler form.

For the straight line, $\dot{r} = \hat{d}$ is constant and $d = |t - t'|$. We get

$$C_0 = G(d), \quad C_1 = -G'(d), \quad C_2 = -G''(d). \tag{18a}$$

For a circle of radius r , define $\alpha \equiv (t - t')/(2r)$, so $d = 2r \sin \alpha$, and by simple geometrical identities, we get

$$\begin{aligned} C_0 &= G(d), & C_1 &= -\cos \alpha G'(d), \\ C_2 &= \sin^2 \alpha \frac{G'(d)}{d} - \cos^2 \alpha G''(d). \end{aligned} \tag{18b}$$

3.1. Normalized correlation for the line and the circle

Substituting (4) in (18a) and (18b), we get the amplitude correlations. The results for the circle are (the straight line is given by their $\alpha \rightarrow 0$ limit)

$$\begin{aligned} C_0 &= J_0(kd) \\ C_1 &= k \cos(\alpha) J_1(kd) \\ C_2 &= k^2 \left(J_0(kd) \cos^2(\alpha) - \frac{J_1(kd)}{kd} \right). \end{aligned} \tag{19}$$

For the density, we substitute $c_2 = C_2(0) = \frac{1}{2}k^2$ in (14) getting $\langle \rho \rangle = k/(\sqrt{2}\pi)$. We use this to select a curve parameter which measures length in units of average spacing (so we can expect meaningful results at the $\langle \rho \rangle \rightarrow \infty$ limit)

$$s \equiv (t' - t)\langle \rho \rangle = (t - t')k/(\sqrt{2}\pi).$$

In the new units, $\alpha = s\sqrt{2}\pi/(2kr)$ and the argument of the Bessel functions is

$$\theta \equiv kd = 2kr \sin\left(\frac{\sqrt{2}\pi s}{2kr}\right) \xrightarrow{kr \rightarrow \infty} \sqrt{2}\pi s.$$

For the NI normalized correlation, we substitute (19) in (17), getting

$$\begin{aligned} \hat{c} &= \frac{[J_0(\theta) \cos^2 \alpha - J_1(\theta)/\theta][1 - J_0(\theta)^2] - J_0(\theta)J_1^2(\theta) \cos^2 \alpha}{[1 - J_0^2(\theta)]/2 - J_1^2(\theta) \cos^2 \alpha} \\ \mathcal{R} &= \frac{1 - J_0^2(\theta) - 2J_1^2(\theta) \cos^2 \alpha}{[1 - J_0^2(\theta)]^{3/2}} (\sqrt{1 - \hat{c}^2} + \hat{c} \arcsin \hat{c}) - 1. \end{aligned} \tag{20}$$

To get the universal distribution (k -independent, high-density limit), we take $k \rightarrow \infty$ keeping s constant:

$$\begin{aligned} \hat{c} &= \frac{[J_0(\theta) - J_1(\theta)/\theta][1 - J_0(\theta)^2] - J_0(\theta)J_1^2(\theta)}{[1 - J_0^2(\theta)]/2 - J_1^2(\theta)} \\ \mathcal{R} &= \frac{1 - J_0^2(\theta) - 2J_1^2(\theta)}{[1 - J_0^2(\theta)]^{3/2}} (\sqrt{1 - \hat{c}^2} + \hat{c} \arcsin \hat{c}) - 1. \end{aligned} \tag{21}$$

Note that in the case of the straight line ($\kappa \equiv 1/r \rightarrow 0$), we have $\theta = \sqrt{2}\pi s$ and $\alpha = 0$ exactly, so there is no k dependence, and the universal function (21) is exact for any k (this is expected, because with no boundary and no curvature, the system has no natural scale).

To further study the universal correlation function (21), we derive its asymptotic expansion. The first few terms in the expansion of $\mathcal{R}(s)$ near $s = 0$ are

$$-1 + \frac{\pi^2}{16}s + \frac{37\pi^4}{2304}s^3 + \frac{\pi^4}{1296\sqrt{2}}s^4. \tag{22}$$

This rises linearly from -1 , with a smaller slope than the GOE ensemble (other RMT ensembles are not linear at this limit); however, as is shown in figure 3, it rises quicker to positive values, resulting in a smaller range of high repulsion.

For large values of s , we find decaying terms, oscillating in frequencies which are multiples of the dominant frequency $\omega \equiv 2\pi\sqrt{2}$. The asymptotic expansion has the form

$$\mathcal{R}(s) \sim \text{Re} \sum_{n=1}^3 \frac{1}{(\pi\omega s)^n} \sum_{m=0}^n q_{n,m}(i\pi) e^{im(\omega s - \pi/2)} + O(s^{-4}), \tag{23}$$

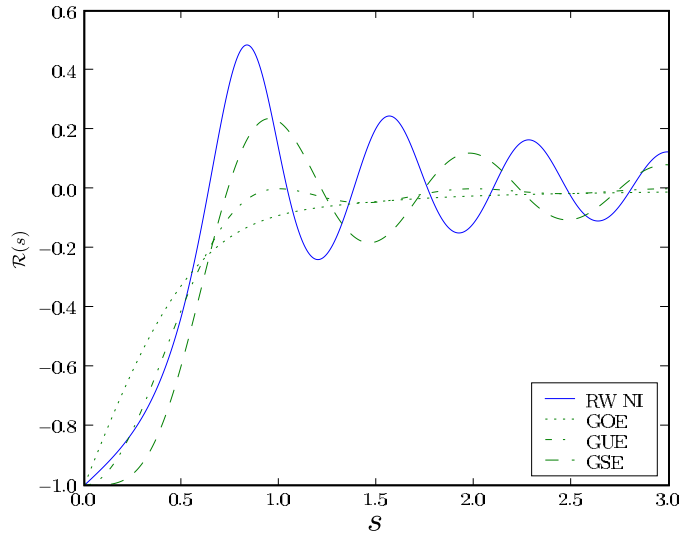


Figure 3. Normalized correlation: NI of RW versus RMT level spacings.

where $q_{n,m}(x)$ are the following polynomials:

$$\begin{aligned}
 q_{1,0} &= 1, & q_{1,1} &= 9 \\
 q_{2,0} &= \frac{25}{4}, & q_{2,1} &= \frac{49}{3} + \frac{39}{2}x, & q_{2,2} &= \frac{121}{12} \\
 q_{3,0} &= \frac{169}{4} + \frac{17}{2}x^2, & q_{3,1} &= \frac{1369}{24} + \frac{511}{6}x + \frac{205}{8}x^2, \\
 q_{3,2} &= \frac{1681}{60} + \frac{55}{12}x, & q_{3,3} &= \frac{529}{40}.
 \end{aligned}$$

Writing the leading terms explicitly, we have

$$\mathcal{R} \sim \frac{1}{\pi\omega s} (1 + 9 \sin(\omega s)). \tag{24}$$

This s^{-1} decay is slower than the decay of random matrix ensembles (s^{-2} for GOE and GUE, and $s^{-1} \times$ [oscillating part] for GSE). The slow decay has a considerable effect on all statistics that probe large distances, as will be shown in section 3.2.

When we look at intersections on a full circle, s goes over all values from $-kr/\sqrt{2}$ to $kr/\sqrt{2}$. This range contains values large enough to make (21) unsuitable for approximating the correlations. The leading terms in the asymptotic expansion of (20) (the equivalent of (24)) are found to be

$$\mathcal{R}(s) = \frac{1}{\pi\Omega_s s} (A_s + B_s \sin(\Omega_s s)) + O(s^{-2}), \tag{25}$$

where

$$A_s = \cos^2\left(\frac{2\pi s}{\sqrt{2}kr}\right), \quad B_s = \left[2 + \cos\left(\frac{2\pi s}{\sqrt{2}kr}\right)\right]^2, \quad \Omega_s = \text{sinc}\left(\frac{s}{\sqrt{2}kr}\right) \cdot \omega$$

(with normalized $\text{sinc}(x) \equiv \sin(\pi x)/(\pi x)$), are slowly varying functions, starting from $A_0 = 1, B_0 = 9$ and $\Omega_0 = \omega$ (as expected from (24), which holds for $s \ll kr$), and ending in $A_{\pm S} = 1, B_{\pm S} = 1$ and $\Omega_{\pm S} = 4\sqrt{2}$ for $S = kr/\sqrt{2}$. The functions A_s, B_s and Ω_s are illustrated in figure 4. As we increase k , the rate of change becomes slower, but the normalized length of the curve increases, and the value of the coefficients for maximally separated points ($|s| = kr/\sqrt{2}$) remains the same.

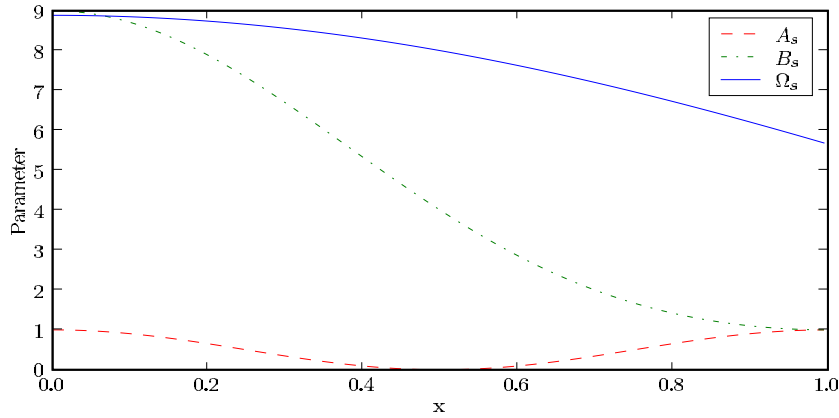


Figure 4. Asymptotic coefficients and frequency for RW NI on half a circle as a function of $x = \sqrt{2}s/(kr)$.

Before proceeding to compute other statistics, we would like to point out that the oscillations in $p(s)$ (see section 2.1) have a frequency which is numerically consistent with half the dominant frequency $\omega \equiv 2\pi\sqrt{2}$.

3.2. Number variance and form factor

The variance of the number of intersections in a finite segment of length L is often used as a measure for the ‘rigidity’ of the distribution (a completely rigid set of points will have zero variance). The correlation form factor (power spectrum [17]) measures periodicity in the distribution (which is also manifested by oscillations in the correlation function). These statistics are given by integral transforms of \mathcal{R} which are hard to solve directly. Instead, the asymptotic expansions of the correlation function can be used to expand them in series at regions of interest, as explained in appendix C.

The variance for the number of intersections on a finite segment of length L can be calculated from the normalized correlation by [20]

$$\Sigma^2(L) = L + 2 \int_0^L (L - s)\mathcal{R}(s) ds. \tag{26}$$

We can use (22) and (23) to find the asymptotic behaviour of this statistics. For small L , we find

$$\Sigma^2 \sim L - L^2 + \frac{\pi^2}{48}L^3 + \frac{37\pi^4}{23040}L^5 + \frac{\pi^4}{19440\sqrt{2}}L^6$$

The first two terms follow from the formal definition of Σ^2 , and therefore coincide with the corresponding terms in the RMT ensembles. The third term corresponds to the probability of finding two intersections in the small interval $[0, L]$. It is of order L^3 , as in GOE (again with a smaller factor).

For large L , we find

$$\begin{aligned} \Sigma^2 \sim & \frac{2q_{1,0}}{(\pi\omega)}(L \ln L - L) + L(1 + 2\mathcal{M}_{\text{RW}}^0) - \frac{2q_{2,0}}{(\pi\omega)^2}(\ln L + 1) - 2\mathcal{M}_{\text{RW}}^1 \\ & + \frac{1}{(\pi\omega)^3L} \text{Re}[q_{3,0}(i\pi) + 2i\pi^2q_{1,1} e^{i\omega L}] + O(L^{-2}), \end{aligned} \tag{27}$$

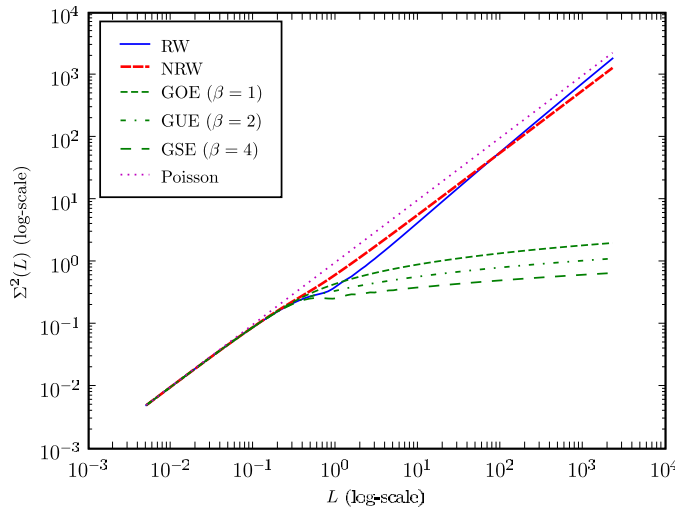


Figure 5. Number variance in segments of length L . For large L , the NRW curve is linear, hence parallel to the Poisson curve. The RW curve rises faster (the crossing point is at $L \sim 32 \times 10^3$, beyond the range of this plot).

where $\mathcal{M}_{\text{RW}}^0$ and $\mathcal{M}_{\text{RW}}^1$ are fixed constants, given by

$$\begin{aligned} \mathcal{M}_{\text{RW}}^0 &= \int_0^1 \mathcal{R}(s) \, ds + \int_1^\infty \left[\mathcal{R}(s) - \frac{1}{\pi \omega s} \right] \, ds \sim -0.336 \\ \mathcal{M}_{\text{RW}}^1 &= \frac{1}{\pi \omega} \left(9 \frac{\cos \omega}{\omega} - 1 \right) + \int_0^1 s \mathcal{R}(s) \, ds \\ &\quad + \int_1^\infty \left[s \mathcal{R}(s) - \frac{1}{\pi \omega} (1 + 9 \sin \omega s) - \frac{25}{4(\pi \omega)^2 s} \right] \, ds \sim -0.0826 \end{aligned}$$

Writing down the first terms of (27) explicitly, we have

$$\Sigma^2(L) \sim \frac{2}{\pi \omega} L \ln L + \left(1 - \frac{2}{\pi \omega} + 2\mathcal{M}_{\text{RW}}^0 \right) L - \frac{25}{(2\pi \omega)^2} \ln L - 2 \left(\mathcal{M}_{\text{RW}}^1 + \frac{25}{(2\pi \omega)^2} \right). \quad (28)$$

Note that this variance is asymptotically larger than that of the random (Poisson) distribution (where $\Sigma^2 \sim L$). However, due to the numerical constants, the $L \ln L$ term dominates only when $L > \exp(\pi \omega (\mathcal{M}_{\text{RW}}^0 + 1/2) - 1) \sim 36$, and only at $L \sim 32 \times 10^3$ does it become larger than the Poisson variance. At segments whose length is a few average spacings, the variance already becomes significantly larger than the ‘rigid’ RMT ensembles. In figure 5, the variances of several distributions are compared.

It should be noted that in the case of independent-site percolation (for grids with bounded, convex cells), a straight line passes only once through each cell. Hence the sign changes along the line form a Poisson process, with linear number variance. The fact that the asymptotic behaviour of the random wave model behaves differently is of interest, because the predictions of the percolation model [5] matched the numerical data for other parameters which characterize the behaviour of RW nodal lines in the high energy limit, namely, the nodal count (number of nodal domains contained inside a given area) [4] and the SLE driving force [19].

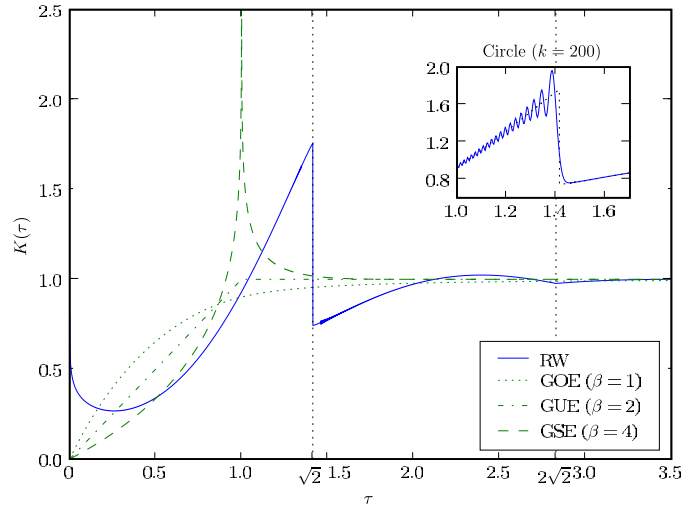


Figure 6. Form factor for RW Nodal intersections. The logarithmic divergence to $+\infty$ at $\tau = 0$ is too steep to be observable in this scale.

The form factor (scaled power spectrum) for the intersections is the Fourier transform of the scaled correlation function (up to the subtraction of a $\delta(\tau)$ term),

$$\begin{aligned}
 K(\tau) &= \int_{\Gamma} e^{i2\pi\tau s} \frac{\langle \rho(x)\rho(x+s) \rangle}{\langle \rho \rangle^2} ds - \delta(\tau) \\
 &= 1 + \int_{\Gamma} e^{i2\pi\tau s} \mathcal{R}(s) ds.
 \end{aligned}
 \tag{29}$$

In figure 6, this is plotted and compared to the corresponding RMT values.

By (24) it is clear that K diverges for $\tau = 0$ (since $1/(\pi\omega s)$ is non-integrable). Similarly, from the form of equation (23), we expect singularities at integer multiples of $\sqrt{2}$ (corresponding to the angular frequency $\omega = 2\pi\sqrt{2}$). To quantify this, we use the asymptotic expansion of \mathcal{R} to expand $K(\tau)$ in small regions around the singular points $\tau = \sqrt{2}n + \delta$ for $\delta \ll 1$.

For the divergence at 0 ($\tau \ll 1$), we get

$$K(\tau) \sim 1 + 2\mathcal{M}_{\text{RW}}^0 - \frac{2[\gamma + \ln(2\pi)]}{\pi\omega} - \frac{2}{\pi\omega} \ln \tau$$

This is a logarithmic divergence. It drops down to 1 at $\tau_0 \sim 8 \times 10^{-6}$ (which is too small to be observable in figure 6). The parameter $K(0) = 1 + \int_{\Gamma} \mathcal{R}(s) ds$ can be viewed as a measure of asymptotic spectral rigidity [23]. In our case, we see that we have ‘infinite softness’—the slow decay of the correlations outweighs the short distance repulsion.

One notable feature of figure 6 is the finite jump at $\tau = \sqrt{2}$. Expanding for this region, we find

$$K(\sqrt{2} + \delta) \sim A + B\delta - \frac{9}{2\omega} \text{Sign}[\delta] - \frac{39}{16\pi} |\delta| + \frac{49}{12\pi^3} \delta \ln |\delta|,$$

where $A \sim 1.25$ and $B \sim 1.53$ are numerical constants.

For the case where the reference line is a circle (inset of figure 6), we observe strong oscillations in the form factor for $\tau < \sqrt{2}$. These oscillations are caused by the ‘drifting’ of the frequency Ω_s in (25). Their frequency increases for large values of k , and we would expect them to cancel out when averaged over a wide enough window of frequencies.

4. The normal derivative of a Gaussian field

When dealing with solutions of boundary value problems (e.g. two-dimensional quantum billiards), the boundary of the domain is a curve that plays a special role. It is therefore worthwhile investigating its intersections with the nodal lines. For a Dirichlet boundary condition, the boundary is a part of the nodal set, and the derivative of the eigenfunction in the tangent direction is zero. At the points where another nodal line intersects the boundary, the derivative in the direction of the other line will also vanish. Since nodal lines of solutions of the Helmholtz equation intersect at right angles, the intersections we wish to explore are also zeros of the *normal derivative* of the field with respect to the curve. This fact makes the normal derivative of other fields, such as the unbound random wave, natural candidates for comparison with the statistics of such intersections.

If fact, the normal derivative of a Gaussian random wave field is directly related to the ‘boundary modified’ field mentioned in section 1. The boundary modified random waves [11], with a correlation function approaching (5), might be realized by symmetrization of the unbound random wave field (2): $\psi_{BRW}(x, y) \equiv \psi(x, y) - \psi(x, -y)$ (where $\psi = \psi_{RW}$ of (4)). In this case, the correlations on the boundary itself can be defined as the limit of correlations on a line parallel to the x axis at $y \rightarrow 0+$. To get a meaningful limit we must introduce a y -dependent scaling, to keep $\langle \psi_{BRW}^2 \rangle$ constant as we approach $y = 0$. Denoting $\phi_y(x) \equiv \psi_{BRW}(x, y)$, the average square amplitude for a line at height y is

$$\langle \phi_y(x)^2 \rangle = \langle (\psi(x, y) - \psi(x, -y))^2 \rangle = 2(c_0 - C_0(2y))$$

The correlation function C_0 is symmetric, so in the generic case (and, in our case specifically), its value for small d can be approximated by a square function $C_0(d) \sim c_0 + \frac{1}{2}c''_0d^2$. Thus, $\langle \phi_y(x)^2 \rangle \sim (2y)^2|c''_0|$ (note that c''_0 is negative), and the scaled field will be

$$\begin{aligned} \widehat{\phi}_y(x) &= \frac{\psi(x, y) - \psi(x, -y)}{\sqrt{\langle \phi_y(x)^2 \rangle}} \\ &\sim \frac{1}{\sqrt{|c''_0|}} \frac{\psi(x, y) - \psi(x, -y)}{2y} \xrightarrow{y \rightarrow 0+} \frac{1}{\sqrt{|c''_0|}} \frac{\partial \psi(x, y)}{\partial y}. \end{aligned}$$

Therefore, the properly scaled boundary modified field is proportional to the normal derivative of the random wave field used to generate it.

4.1. Amplitude correlations of the normal derivative on the reference curve

The normal derivative of the field across the curve is given by $g(t) = \mathbf{n}(t) \cdot \nabla \psi(\mathbf{r}(t))$, where $\mathbf{n}(t)$ is the unit normal vector of the curve at point t . Repeating the computation described in section 2.3, we can calculate its correlation functions:

$$\begin{aligned} \langle g(t)g(t') \rangle &= \sum_{i,j} n_i \frac{\partial^2 \langle \psi(\mathbf{r}(t))\psi(\mathbf{r}(t')) \rangle}{\partial r_i \partial r'_j} n'_j \\ &= \sum_{i,j} -n_i \left[\left(G''(d) - \frac{G'(d)}{d} \right) \frac{d_i d_j}{d^2} + \frac{G'(d)}{d} \delta_{ij} \right] n'_j. \end{aligned} \tag{30}$$

For the circle (as before $\alpha = (t - t')/(2r)$, $d = 2r \sin \alpha$), we have the identities $\mathbf{n} \cdot \mathbf{n}' = \cos(2\alpha)$ and $\mathbf{n}' \cdot \hat{\mathbf{d}} = -\mathbf{n} \cdot \hat{\mathbf{d}} = \sin \alpha$. Inserting these in (30) we get

$$C_0 = \langle gg' \rangle = -\cos^2 \alpha \frac{G'(d)}{d} + \sin^2 \alpha G''(d). \tag{31a}$$

The other two correlation functions are calculated in a similar manner (for a general curve) in appendix B. For the case where the curve is a circle, they assume the following form²:

$$C_1 = \langle g \dot{g}' \rangle = \cos \alpha (1 - 3 \sin^2 \alpha) \left(\frac{G''}{d} - \frac{G'}{d^2} \right) - \sin^2 \alpha \cos \alpha \left(G^{(3)} + 4 \frac{G'}{d^2} \right) \quad (31b)$$

$$C_2 = \langle \dot{g} \dot{g}' \rangle = -2 \left(\cos(2\alpha) + \frac{7}{8} \sin^2(2\alpha) \right) \frac{1}{d^2} \left(G'' - \frac{G'}{d} \right) + \left(1 - \frac{3}{2} \sin^2(2\alpha) \right) \frac{G^{(3)}}{d} - \sin^2 \alpha \left(\cos^2 \alpha G^{(4)} + 4 \cos(2\alpha) \frac{G'}{d^3} \right). \quad (31c)$$

The correlations for the straight line are easily derived from equations (31a)–(31c) by taking the limit $\alpha \rightarrow 0$:

$$C_0 = -\frac{G'}{d} \quad (32a)$$

$$C_1 = \frac{G''}{d} - \frac{G'}{d^2} \quad (32b)$$

$$C_2 = \frac{G^{(3)}}{d} - \frac{2}{d^2} \left(G'' - \frac{G'}{d} \right). \quad (32c)$$

To study the normally derived field corresponding to the monochromatic random ensemble of section 3, we apply the results above to the specific correlation function, and discuss the resulting statistics. For simplicity, we discuss the case of a straight line first, and follow with comments about the main differences in the case of a circular curve.

For the straight line, the amplitude correlations are derived from (32a)–(32c). To get a standard scaling with $c_0 = 1$, we first multiply the field by $\sqrt{2}/k$, getting $G = 2J_0(kd)/k^2$, and the following correlations for the normal derivative:

$$\begin{aligned} C_0 &= \frac{2J_1(kd)}{kd} \\ C_1 &= k \frac{2J_2(kd)}{kd} \\ C_2 &= k^2 \frac{2}{kd} \left(\frac{J_2(kd)}{kd} - J_3(kd) \right). \end{aligned} \quad (33)$$

4.2. Nodal intersection statistics for a straight line

We proceed as in section 3. First, the density of intersection is calculated using (14):

$$\langle \rho \rangle = \frac{1}{\pi} \sqrt{\frac{c_2}{c_0}} = \frac{k}{2\pi}.$$

We use this to rescale the distance to units of average spacing $s = (t - t')k/(2\pi)$, so the argument of the Bessel functions in (33) becomes $\theta = 2\pi s$. Substituting these results in (17), we get

$$\begin{aligned} \hat{c} &= \frac{8 (J_2 - \theta J_3)(\theta^2 - 4J_1^2) - 4\theta J_1 J_2^2}{\theta^2 (\theta^2 - 4J_1^2 - 16J_2^2)} \\ \mathcal{R} &= \frac{\theta(\theta^2 - 4J_1^2 - 16J_2^2)}{(\theta^2 - 4J_1^2)^{3/2}} (\sqrt{1 - \hat{c}^2} - \hat{c} \arcsin \hat{c}) - 1. \end{aligned} \quad (34)$$

² This form was chosen to make the $\alpha \rightarrow 0$ limit more evident. The forms in appendix B are more suitable for calculations involving Bessel functions or generic derivatives.

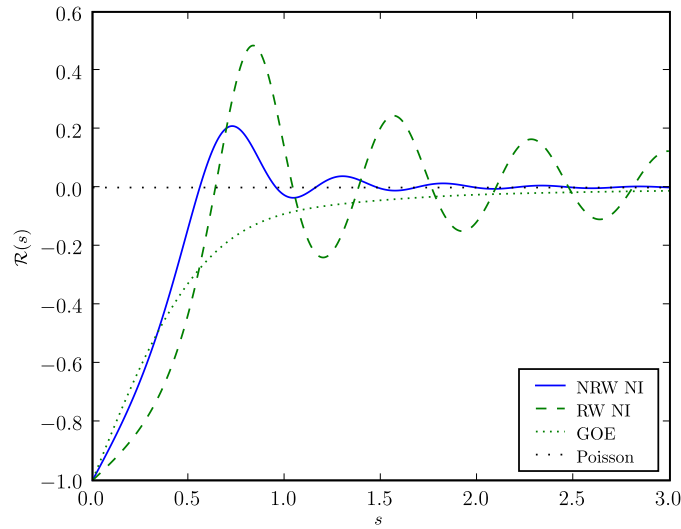


Figure 7. Normalized correlation: NI of normally derived RW.

The asymptotic expansion of \mathcal{R} for small s is

$$\mathcal{R}(s) \sim -1 + \frac{\pi^2}{8}s + \frac{13\pi^4}{576}s^3 + \frac{\pi^4}{324}s^4.$$

As before, this grows linearly from -1 . The slope is larger than that of the unmodified RW, but smaller than the slope of the GOE correlations. As shown in figure 7, it rises quickly to positive values.

The expansion for large s is

$$\begin{aligned} \mathcal{R}(s) \sim & \frac{2}{\pi(2\pi s)^3} (9 - 25 \sin(4\pi s)) + \frac{-555}{2\pi(2\pi s)^4} \cos(4\pi s) \\ & + \frac{1}{2\pi(2\pi s)^5} \left(-\frac{69}{2} + \frac{12789}{8} \sin(4\pi s) \right). \end{aligned} \tag{35}$$

$\mathcal{R}(s)$ decays as s^{-3} , which is faster than the decay of the correlations for the corresponding RMT ensembles. As in (23), each asymptotic term has oscillating parts, with frequencies which are multiples of the dominant frequency $\omega_{\text{NRW}} = 4\pi$. As in section 3.1, we find that the oscillations in the nearest neighbour density of the NRW, described in section 2.1, have a frequency which is numerically consistent with half the dominant frequency $\omega \equiv 4\pi$.

With the s^{-3} decay of the correlations, both $\int \mathcal{R}(s) ds$ and $\int s\mathcal{R}(s) ds$ are finite, so from (26) it is evident that Σ^2 should increase linearly for large values of L . The asymptotic expansion calculated from (35) is

$$\Sigma^2 \sim (1 + 2\mathcal{M}_{\text{NRW}}^0)L - 2\mathcal{M}_{\text{NRW}}^1, \tag{36}$$

with

$$\mathcal{M}_{\text{NRW}}^0 = \int_0^\infty \mathcal{R}(s) ds \sim -0.2582$$

and

$$\mathcal{M}_{\text{NRW}}^1 = \int_0^\infty s\mathcal{R}(s) ds \sim -0.00617.$$

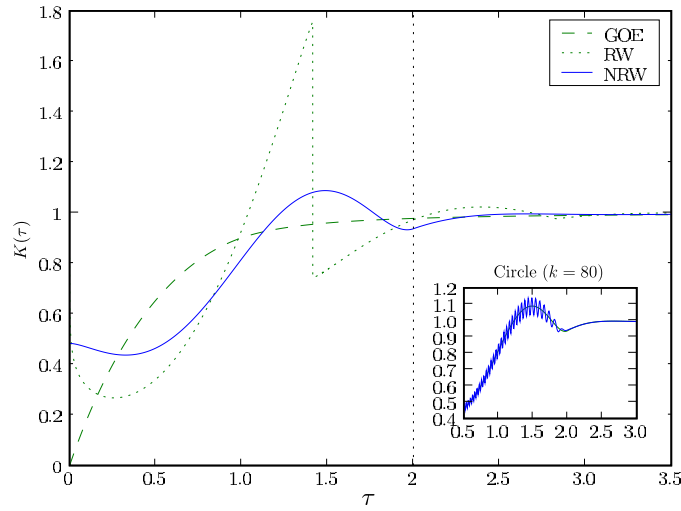


Figure 8. Form factor for the NI of normally derived RW.

As seen in figure 5, the asymptotic variance is larger than RMT ensembles, but smaller than Poisson.

Much in the same way, from (29), it is evident that the form factor (figure 8) will now be finite at $\tau = 0$, and will be continuously differentiable for $\tau > 0$. Irregularities appear in second and higher derivatives at multiples of the dominant frequency ω_{NRW} (i.e. $\tau_n = n\omega_{NRW}/(2\pi) = 2n$). The asymptotic expansion for $\tau \ll 1$ is given by

$$K(\tau) \sim (1 + 2\mathcal{M}_{NRW}^0) + \frac{9}{\pi^2}\tau^2 \ln \tau + \tau^2 \left[\frac{9}{\pi^2} \left(\gamma - \frac{3}{2} + \ln 2\pi \right) - (2\pi)^2 \mathcal{M}_{NRW}^2 \right]$$

with

$$\mathcal{M}_{NRW}^2 = \int_0^1 s^2 \mathcal{R}(s) ds + \int_1^\infty s^2 \left(\mathcal{R}(s) - \frac{9}{4\pi^4 s^3} \right) ds \sim 0.00579.$$

We now have a finite $K(0) \sim 0.4836$. This value is smaller than the $K = 1$ of the Poisson distribution, but larger (softer) than the RMT ensembles, for which $K(0) = 0$.

4.3. Statistics on a circular arc

The case where the reference curve is a circle can be treated similarly. The amplitude correlations of the monochromatic waves (corrected form for (33)) can be calculated directly from (B.5). It should be noted that the amplitude variance $c_0 = C_0(0)$ remains $\frac{1}{2}k^2$ (as for the straight line). However, for any finite k , the variance of the derivative (c_2) is different than the value obtained for the straight line, and induces a larger density of intersections.

The corrected density of intersections for the circle is

$$\rho \equiv \frac{\tilde{k}}{2\pi} = \frac{\sqrt{k^2 + (2\kappa)^2}}{2\pi} \sim \frac{k}{2\pi} \left[1 + 2\left(\frac{\kappa}{k}\right)^2 \right].$$

The $O(\kappa^2)$ increase in density, which is due to curvature, affects the choice of the scaled curve parameter $s = \rho \cdot (t - t')$ and thus all the correlation formulae. It is convenient to express the resulting statistics in terms of the dimensionless parameter

$$\beta = \frac{k}{\tilde{k}} = \frac{kr}{\sqrt{(kr)^2 + 4}},$$

which goes to 1 when $kr \rightarrow \infty$. With this, the small s expansion of the normalized correlation is

$$\mathcal{R} \sim -1 + \frac{\pi^2}{8}\beta^2(11 - 10\beta^2)s + \frac{\pi^4}{576}\beta^2(-24 + 357\beta^2 - 820\beta^4 + 500\beta^6)s^3.$$

For large values of s (the circle is finite, and $|s|$ can only get values up to $\frac{1}{2}\tilde{k}r = (1 - \beta^2)^{-1/2}$), the constant dominant frequency $\omega = 4\pi$ of (36) is replaced with a drifting frequency (changing very slowly with s)

$$\Omega_s = 4\pi\beta \operatorname{sinc}\left(\frac{s}{\tilde{k}r}\right),$$

similar to the situation in section 3.1. However, in the case of the normally derived field, there is another notable difference between the circular and the straight curve. Namely, for any finite value of kr , we get $O(s^{-1})$ and $O(s^{-2})$ terms, which do not appear in the case of a straight line. The leading term of the normalized correlation for $s \gg 1$ is

$$4 \sin^4 \alpha [(4\beta^2 \cos^2 \alpha - 1)^2 - (4\beta^2 \cos^2 \alpha + 1)^2 \sin(\Omega_s s)] \cdot \frac{1}{\pi \Omega_s s},$$

where $\alpha = \pi s / (\tilde{k}r)$ is slowly varying up to $\pi/2$. When we are in the $1 \ll s \ll \tilde{k}r$ region, α is very small, and this term is $O(\alpha^4)$. Hence, it vanishes in the straight line limit. The $O(s^{-2})$ term, contains the frequencies 0, Ω_s and $2\Omega_s$. In the low α region, it is $O(\alpha^2 \cos(\Omega_s s) (\pi \Omega_s s)^{-2})$ (again, vanishes for the straight line). The $O(s^{-3})$ term is the first one that does not vanish when $\alpha \rightarrow 0$.

The effect of these terms is manifested by the number variance statistic. In figure 9, the number variance is plotted for three values of kr . As long as $L \ll \tilde{k}r$, the variance stays close to the values corresponding to a straight curve given by (36). However, when the angle covered by the segment becomes non-negligible, $O(\alpha^4 s^{-1})$ and $O(\alpha^2 s^{-2})$ terms of the correlation become important, and the variance increases above the linear asymptote.

5. Comparison with other fields

The statistics considered above can be evaluated numerically for the nodal intersections of any scalar field with a given reference curve. If a random Gaussian model is given for the field, the techniques demonstrated above can be used to extract the theoretical functions predicted by the model, and those could be compared to the numerical results. This gives a useful tool for verifying statistical models for such systems. For the case of chaotic billiards, the numerical results can be compared to the predictions of random wave models. Also, we can use these statistics to compare other random wave models with the monochromatic random waves. In [14], the field with correlation (7) was compared to the random waves model with respect to special statistics proposed there (which were related to the probability of finding a nodal line inside a reference tube). The nodal intersection statistics provide another way to compare these models.

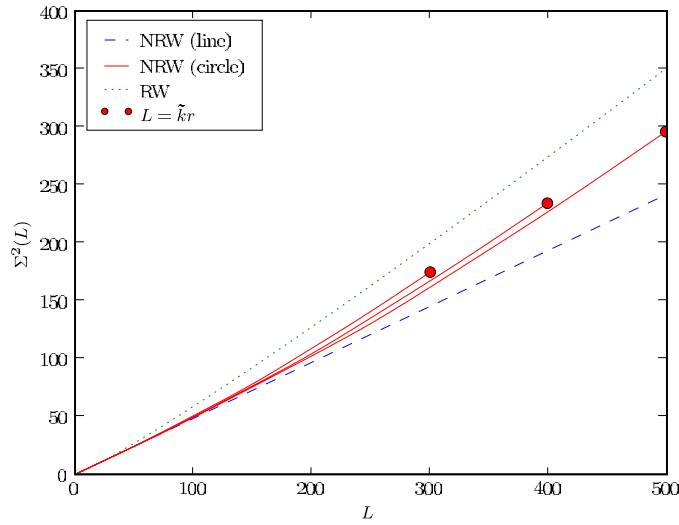


Figure 9. Number variance for zeros of NRW on a circular curve, for three different values of kr . The length of the segment is bound by the total length of the circle, marked by circular dots on the plot.

5.1. The Gaussian short-range field

The short-range field (7) was chosen so that its short distance behaviour will be the same as that of the monochromatic random wave field, so we expect the average level spacing to be $\sqrt{2\pi}/k$. Substituting the correlation function (7) in (18b), and denoting $G = \exp(-\theta^2/4)$, $\theta = kd$, we get

$$C_0 = G, \quad C_1 = \frac{1}{2}k\theta \cos(\alpha)G,$$

$$C_2 = \frac{1}{2}k^2 \left[\cos(2\alpha) - \frac{1}{2}\theta^2 \cos^2(\alpha) \right] G$$

(so $c_2 = k^2/2$ as expected, and $\theta \rightarrow \sqrt{2\pi}s$ as before). The nodal intersections correlation for the straight line becomes

$$\hat{c} = e^{-\frac{1}{4}\theta^2} \frac{1 - e^{-\frac{1}{2}\theta^2} - \frac{1}{2}\theta^2}{1 - e^{-\frac{1}{2}\theta^2} - \frac{1}{2}\theta^2 e^{-\frac{1}{2}\theta^2}} \tag{37}$$

$$\mathcal{R}(s) = \frac{1 - e^{-\frac{1}{2}\theta^2} - \frac{1}{2}\theta^2 e^{-\frac{1}{2}\theta^2}}{(1 - e^{-\frac{1}{2}\theta^2})^{\frac{3}{2}}} (\sqrt{1 - \hat{c}^2} + \hat{c} \arcsin(\hat{c})) - 1.$$

The expansion for small s is

$$\mathcal{R} \sim -1 + \frac{\pi^2}{4}s - \frac{\pi^4}{48}s^3 + \frac{\sqrt{3}\pi^4}{54}s^4 + O(s^5),$$

and for large s , it is

$$\mathcal{R} \sim e^{-(\pi s)^2} \left[\frac{1}{2}(\pi s)^4 - 2(\pi s)^2 + 1 \right] + O(e^{-2(\pi s)^2} s^8).$$

As can be seen in figure 10(a), the slope at 0 is higher than that of the GOE, and the correlations decay to 0 faster than all other distributions considered here. Thus, this field has smaller repulsion and it may be considered the closest to the random Poisson distribution.

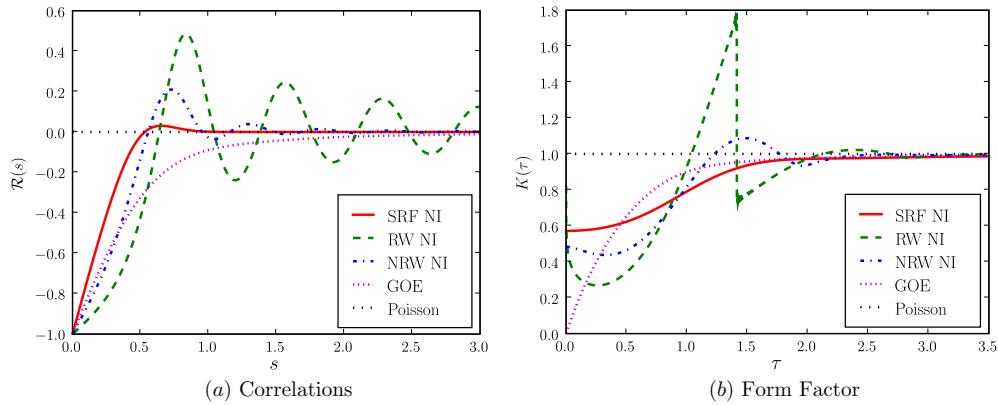


Figure 10. SRF nodal intersections compared to other fields.

The number variance and form factor also reflect this property. Denoting

$$\begin{aligned} \mathcal{M}_{\text{SRF}}^0 &= \int_0^\infty \mathcal{R}(s) \, ds \sim -0.2141 \\ \mathcal{M}_{\text{SRF}}^1 &= \int_0^\infty s \mathcal{R}(s) \, ds \sim -0.02902 \\ \mathcal{M}_{\text{SRF}}^2 &= \int_0^\infty s^2 \mathcal{R}(s) \, ds \sim -0.00434, \end{aligned}$$

we find that the asymptotic number variance is linear with coefficient $(1 + 2\mathcal{M}_{\text{SRF}}^0) \sim 0.5718$, which is larger than the normally derived random waves (thus closer to Poisson).

The form factor has a smooth form (because (37) is not oscillatory). The expansion for small τ is

$$K(\tau) \sim (1 + 2\mathcal{M}_{\text{SRF}}^0) - 4\pi^2 \mathcal{M}_{\text{SRF}}^2 \tau^2.$$

We get a relatively large $K(0) \sim 0.5718$, and a quick approach to the limiting value of 1 (which is consistent with the notion that this is closer to the Poisson distribution).

5.2. Chaotic billiards

Eigenfunctions of chaotic billiards provide an ensemble of functions with complex behaviour. In the semiclassical limit, they are well modelled by Gaussian random wave ensembles (the monochromatic random wave ensemble is used to model the eigenfunctions in regions which are far enough from the boundary, and various boundary modified ensembles model the field close to the boundary).

The statistics considered in this paper were evaluated numerically for eigenfunctions of desymmetrized Bunimovich stadium (0.5×1 rectangle joined with a quarter of a circle of radius 1) and desymmetrized Sinai billiard (1.2×1 rectangle, with a quarter of a circle of radius 0.5 cut out of one of the corners)—both with Dirichlet boundary conditions. For the Stadium, 1500 eigenfunctions were taken, with wave numbers ranging from $k = 110$ to $k = 165$. For the Sinai billiard, we used 10 000 wavefunctions, with wave numbers from 350 to 500.

Fixed reference curves were chosen in the interior of the billiards, as shown in figure 11. For each wavefunction, the sequence of intersections of the nodal lines with these curves was calculated, and normalized to unit average spacing according to the corresponding

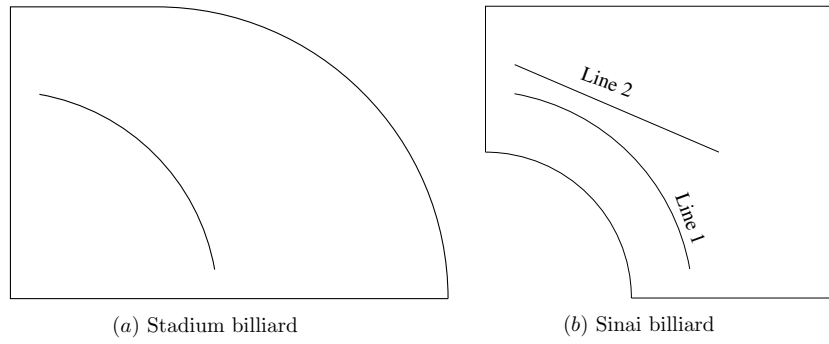


Figure 11. Internal reference curves in the quantum billiards.

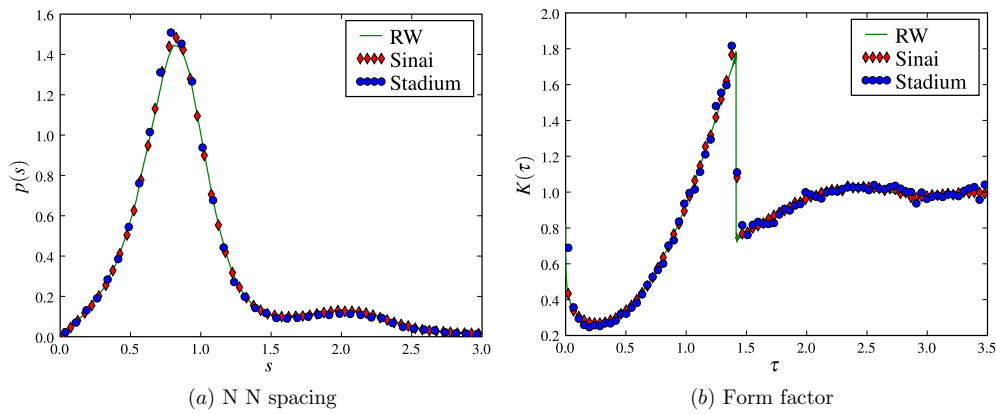


Figure 12. Billiards: NI with internal line.

wavenumber. As shown in figure 12, the nearest neighbour distribution agrees very well with the predictions of the random waves model. The form factor is also very close to the expected curve.

The number variance of nodal intersections on segments of the reference curves is plotted in figure 13. For short segments, the results are close to the predictions of the random waves model, but deviate considerably from this model as we move to segments of large normalized length, especially in the case of the Sinai billiard. This deviation happens when the (unscaled) length of the segment is comparable to the billiard dimensions. On such scales, it seems likely that the geometrical details of the billiard would have an effect on the statistical properties of the wavefunctions.

6. Summary

The analytic results obtained for the three Gaussian fields discussed in this paper are summarized in table 1, and compared to their analogues in the well-known random matrix and Poisson ensembles. For short distances, the normalized correlation function for all the distributions considered (except of the Poisson distribution) approaches -1 , so the leading term of $1 + \mathcal{R}(s)$ is listed, for $s = \epsilon \ll 1$. Similarly, the number variance for short

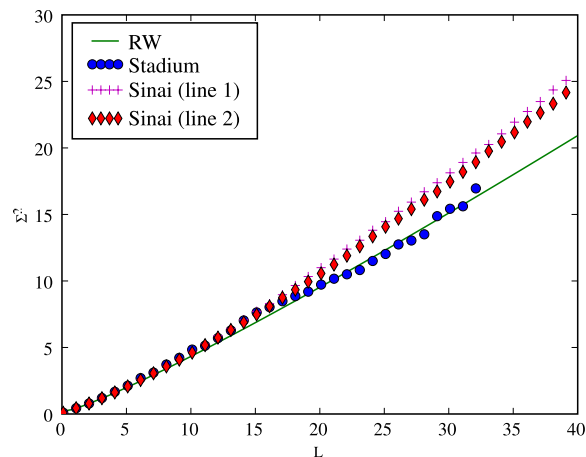


Figure 13. Number variance of NI with segments inside chaotic billiards.

intervals is asymptotically $L - L^2$ (again, except of the Poisson case), so the leading term of $\hat{\mathcal{R}}_2 = \Sigma^2(L) - L + L^2 = E[n(n-1)]$ is listed. (For $L = \epsilon \ll 1$, this is also twice the probability of finding two points in the interval). For large distances, we list the leading terms of Σ^2 and \mathcal{R} . For the form factor, we list the ‘asymptotic rigidity’ $K(0)$ (which is directly related to Σ^2 and $\bar{\Delta}$ in large intervals [20, 23]), the singular frequencies where $K(\tau)$ or its derivatives diverge and the type of divergence (number of the first diverging derivative) in the first nonzero singular frequency.

We have seen that

- Nodal intersections (NI) with a reference curve can be used as a statistical means to obtain insight into the properties of complex networks of lines. The NI statistics of the random wave (RW) model display characteristic behaviour, which is quite different from the statistics of other point processes. Eigenfunctions of chaotic billiards match these statistics well, with some differences on scales comparable to the dimensions of the billiard.
- For the RW and some other Gaussian models, the two-point correlations and other statistics related to it can be derived by analytical means.
- The nearest neighbour distribution is harder to obtain (since it depends on n -point correlations with $n \geq 3$). However, numerical evidence suggests that the frequency of oscillations is related to the dominant frequencies calculated for the corresponding two-point correlation functions.

Acknowledgments

This research was initiated as a result of a conversation with Percy Deift, whose interest and help accompanied us throughout the work. Thanks Percy! We would like to acknowledge Sven Gnutzmann for valuable discussion and for the Stadium billiard data, Zeev Rudnick and Mark Dennis for important references. We thank Holger Schanz for the Sinai billiard data, and Yehonatan Elon for careful reading of the text and useful comments. The work was supported by the Minerva Center for non-linear Physics and the Einstein (Minerva) Center at the Weizmann Institute, and by grants from the GIF (grant I-808-228.14/2003), and EPSRC (grant GR/T06872/01.) and a Minerva grant.

Table 1. Comparison of NI statistics.

Process	Correlation		Form factor		Number variance	
	$1 + \mathcal{R}(\epsilon)$	$\mathcal{R}(s \gg 1)$	$K(0)$	Divergences ^a	$\hat{R}_2(\epsilon)$	$\Sigma^2(L \gg 1)$
Poisson	1	0	1	—	ϵ^2	L
SRF	2.467ϵ	$48.7s^4 e^{-(\pi s)^2}$	0.572	—	$0.822\epsilon^3$	$0.572L$
NRW	1.234ϵ	$0.023s^{-3}$	0.484	⁽³⁾ {2, 4, ...}	$0.411\epsilon^3$	$0.484L$
RW	0.617ϵ	$0.036s^{-1}$	∞	⁽¹⁾ { $\sqrt{2}, 2\sqrt{2}, \dots$ }	$0.206\epsilon^3$	$0.072L \log L$
GOE	1.645ϵ	$-0.101s^{-2}$	0	⁽⁴⁾ {1}	$0.548\epsilon^3$	$0.203 \log L$
GUE	$3.290\epsilon^2$	$-0.051s^{-2}$	0	⁽²⁾ {1}	$0.548\epsilon^4$	$0.101 \log L$
GSE	$11.55\epsilon^4$	$0.25s^{-1} \cos(\omega s)$	0	⁽⁰⁾ {1, 2}	$0.770\epsilon^6$	$0.051 \log L$

^a Nonzero values of τ , for which $K(\tau)$ or one of its derivatives diverge. The number in parentheses specifies the diverging derivative at the first of these points.

Appendix A. Derivation of the zeros correlation from amplitude statistics

In section 2.4, the correlation of the zeros of a Gaussian random function on a curve was expressed in terms of the Fourier integral (15):

$$\langle \rho \rho' \rangle = \left\langle \frac{1}{4\pi^4} \int \frac{d\xi d\eta d\xi' d\eta'}{\eta^2 \eta'^2} e^{i\xi f} (1 - e^{i\eta f'}) e^{i\xi' f'} (1 - e^{i\eta' f'}) \right\rangle.$$

We note that the integrand contains four terms of the form $\exp(i\mathbf{v}_i \cdot \mathbf{f})$, with

$$\mathbf{v}_i \in \{(\xi, \xi', 0, 0), (\xi, \xi', \eta, 0), (\xi, \xi', 0, \eta'), (\xi, \xi', \eta, \eta')\},$$

and $\mathbf{f} = (f, f', \dot{f}, \dot{f}')$.

If we use (13) to evaluate the statistical average, these terms are replaced by $\exp(-\frac{1}{2} \mathbf{v}_i^T M \mathbf{v}_i)$, where M is the covariance matrix of \mathbf{f} , given in (16). To continue, we first integrate the ξ and ξ' coordinates. To separate them out, we use a simple block matrix identity.

For any pair of column vectors $\mathbf{x}, \mathbf{y} \in \mathbb{R}^n$ and three $n \times n$ matrices A, B, C , where A and B are symmetric and A is non-singular, the following identity can be simply derived:

$$(\mathbf{x}^T \mathbf{y}^T) \begin{pmatrix} A & C \\ C^T & B \end{pmatrix} \begin{pmatrix} \mathbf{x} \\ \mathbf{y} \end{pmatrix} = (\mathbf{x}^T + \tilde{\mathbf{y}}^T) A (\mathbf{x} + \tilde{\mathbf{y}}) + \mathbf{y}^T \tilde{B} \mathbf{y}, \tag{A.1}$$

where $\tilde{B} = B - C^T A^{-1} C$ and $\tilde{\mathbf{y}} = A^{-1} C \mathbf{y}$.

In addition, using the same notation, one can also deduce the determinant identity

$$\det \begin{pmatrix} A & C \\ C^T & B \end{pmatrix} = \det A \det \tilde{B}, \tag{A.2}$$

which we shall use below.

Applying (A.1) to the four terms, with $\mathbf{v}_i^T = (\mathbf{x}^T, \mathbf{y}_i^T)$ (i.e. $\mathbf{x}^T = (\xi, \xi')$ and $\mathbf{y}_i^T \in \{(0, 0), (\eta, 0), (0, \eta'), (\eta, \eta')\}$), the \mathbf{x} -dependent integration for each of the four terms reduces to the usual Gaussian form

$$\int d\xi d\xi' e^{-\frac{1}{2}(\mathbf{x}^T + \tilde{\mathbf{y}}_i^T) A (\mathbf{x} + \tilde{\mathbf{y}}_i)} = \frac{2\pi}{\sqrt{\det A}}.$$

This does not depend on \mathbf{y} and therefore contributes to a constant multiplicative factor. The remaining integral assumes the following form:

$$\int \int_{-\infty}^{\infty} \frac{d\eta d\eta'}{\eta^2 \eta'^2} (1 - e^{-\frac{1}{2} a \eta^2} - e^{-\frac{1}{2} b \eta'^2} + e^{-\frac{1}{2} \mathbf{y}_2^T \tilde{B} \mathbf{y}_2})$$

(using a, b and c for the matrix elements of \tilde{B}).

This can be rewritten as $I_1 + I_2$, where

$$I_1 = \int \int_{-\infty}^{\infty} \frac{d\eta d\eta'}{\eta^2 \eta'^2} (1 - e^{-\frac{1}{2}a\eta^2})(1 - e^{-\frac{1}{2}b\eta'^2}) = 2\pi\sqrt{ab}$$

and

$$I_2 = \int \int_{-\infty}^{\infty} \frac{d\eta d\eta'}{\eta^2 \eta'^2} e^{-\frac{1}{2}(a\eta^2 + b\eta'^2)} (e^{-c\eta\eta'} - 1).$$

I_2 is not well defined, but taking the Cauchy principal value for the integrals, anti-symmetric integrands do not contribute. After symmetrization and change of integration variables, we get

$$I_2 = \sqrt{ab} \int \int_{-\infty}^{\infty} \frac{dx dy}{x^2 y^2} e^{-\frac{1}{2}(x^2 + y^2)} [\cosh(\hat{c}xy) - 1],$$

with $\hat{c} \equiv c/\sqrt{ab}$. One way to solve this integral is to derive the expression by \hat{c} twice, and integrate back after the x and y integrations. Another way is to express $f(xy) \equiv (xy)^{-2}[\cosh(\hat{c}xy) - 1]$ as a power series in $(xy)^2$, and integrate term by term (each term becomes a square of a simple Gaussian moment). Either way, for any $|\hat{c}| < 1$, we get

$$I_2 = 2\pi\sqrt{ab}[-1 + \sqrt{1 - \hat{c}^2} + \hat{c} \arcsin \hat{c}].$$

To show that the convergence condition $|\hat{c}| < 1$ holds, we note that

$$|\hat{c}| < 1 \Leftrightarrow \det \tilde{B} = ab - c^2 > 0.$$

However, from (A.2) we have $\det M = \det A \det \tilde{B}$. Since both A and M are covariance matrices, they are positive definite, and their determinant must be positive for any non-degenerate case. This can only be consistent if $\det \tilde{B}$ is positive too.

Inserting I_1 and I_2 into the expression for the normalized correlation we find (17)

$$\mathcal{R}(t, t') = \frac{c_0}{c_2} \frac{a}{(\det A)^{3/2}} (\sqrt{1 - \hat{c}^2} + \hat{c} \arcsin(\hat{c})) - 1.$$

Appendix B. Calculating the amplitude correlations for the normal derivative of a Gaussian field

When the investigated field is translationally invariant and isotropic, the correlation functions C_0, C_1 and C_2 for the ‘normally derived’ function $g(t) = \mathbf{n}(t) \cdot \nabla \psi(\mathbf{r}(t))$ can be calculated in terms of the curve parameters and reduced correlation function $G(d)$. The derivation is straightforward but tedious, and follows the same mechanism used in sections 2.3 and 4.1. In this section we recite the main steps and results.

As in previous sections, we start by using linearity to move the derivatives out of the statistical average, getting (30) for the first correlation function C_0 . This expression involves second-order partial derivatives of the basic correlation $\langle \psi \psi' \rangle$, so the expressions for C_1 and C_2 involve third- and fourth-order partial derivatives correspondingly.

Using shorthand notation where tagged parameters refer to values at t' , $\partial_i \equiv \partial/\partial r_i$ and $\partial'_i \equiv \partial/\partial r'_i$, we have

$$\begin{aligned} C_0 &= \sum_{i,j} n_i n'_j \partial_i \partial'_j G(|\mathbf{r} - \mathbf{r}'|) \\ C_1 &= \sum_{i,j} \partial'_i n_i n'_j \partial_i \partial'_j G \\ C_2 &= \sum_{i,j} \partial_i \partial'_i n_i n'_j \partial_i \partial'_j G. \end{aligned} \tag{B.1}$$

The derivatives of n in these expressions can be evaluated using the Frenet formula $\partial_t n = -\kappa \dot{r}$ (where κ is the curvature at t), and the partial derivatives of G can be expressed in terms of derivatives with respect to d (G' , G'' , $G^{(3)}$, $G^{(4)}$) and the distance vector d .

First, we calculate the partial derivatives of G using the following rules for derivatives of the distance $d \equiv |d|$ and direction vector $\hat{d} \equiv d/d$ (where $d = r - r'$):

$$\partial_i d = -\partial'_i d = \hat{d}_i \quad \partial_i \hat{d}_j = -\partial'_i \hat{d}_j = \frac{1}{d}(\delta_{ij} - \hat{d}_i \hat{d}_j).$$

To express the results in a manifestly symmetric way, we define $d_{i_1, i_2, \dots, i_N}^{[k]}$, the ' N -dimensional symmetric direction tensor of degeneracy k ' as the symmetrized product of k Kronecker deltas and $N - 2k$ direction vectors \hat{d} . Specifically,

$$\begin{aligned} d_{ij}^{[0]} &= \hat{d}_i \hat{d}_j, & d_{ij}^{[1]} &= \delta_{ij} \\ d_{ijk}^{[1]} &= \delta_{ij} \hat{d}_k + \delta_{ik} \hat{d}_j + \delta_{jk} \hat{d}_i \\ d_{ijkl}^{[1]} &= \delta_{ij} \hat{d}_k \hat{d}_l + \delta_{ik} \hat{d}_j \hat{d}_l + \delta_{il} \hat{d}_j \hat{d}_k + \delta_{jk} \hat{d}_i \hat{d}_l + \delta_{jl} \hat{d}_i \hat{d}_k + \delta_{kl} \hat{d}_i \hat{d}_j \\ d_{ijkl}^{[2]} &= \delta_{ij} \delta_{kl} + \delta_{ik} \delta_{jl} + \delta_{il} \delta_{jk}. \end{aligned}$$

We also introduce the notation $G^{[n]}$ for the specific combinations of derivatives of G up to order n , which satisfy the following recurrence relations³:

$$\begin{aligned} G^{[0]}(d) &= G(d) \\ G^{[n+1]}(d) &= G^{[n]'}(d) - \frac{n}{d} G^{[n]}(d). \end{aligned}$$

Specifically, we have

$$\begin{aligned} G^{[1]} &= G' \\ G^{[2]} &= G'' - \frac{1}{d} G' \\ G^{[3]} &= G^{(3)} - \frac{3}{d} G'' + \frac{3}{d^2} G' \\ G^{[4]} &= G^{(4)} - \frac{6}{d} G^{(3)} + \frac{15}{d^2} G'' - \frac{15}{d^3} G'. \end{aligned}$$

With these notations, the partial derivatives of G are given by

$$\begin{aligned} \partial_i G &= G^{[1]} d_i^{[0]} \\ \partial_i \partial_j G &= G^{[2]} d_{ij}^{[0]} + \frac{1}{d} G^{[1]} d_{ij}^{[1]} \\ \partial_i \partial_j \partial_k G &= G^{[3]} d_{ijk}^{[0]} + \frac{1}{d} G^{[2]} d_{ijk}^{[1]} \\ \partial_i \partial_j \partial_k \partial_l G &= G^{[4]} d_{ijkl}^{[0]} + \frac{1}{d} G^{[3]} d_{ijkl}^{[1]} + \frac{1}{d^2} G^{[2]} d_{ijkl}^{[2]}. \end{aligned}$$

Substituting these in (B.1), we get

$$\begin{aligned} C_0 &= \sum_{i,j} -n_i n'_j (G^{[2]} d_{ij}^{[0]} + \frac{1}{d} G^{[1]} d_{ij}^{[1]}) \\ &= -(n \cdot \hat{d})(n' \cdot \hat{d}) G^{[2]} - (n \cdot n') \frac{1}{d} G^{[1]}, \end{aligned} \tag{B.2}$$

³ These relations are almost identical to the Bessel recurrence relations. Hence, for the case where $G(d) = J_0(kd)$, we get $G^{[n]} = (-k)^n J_n(kd)$.

which is equivalent to (30). Similarly,

$$\begin{aligned}
 C_1 &= \sum_{i,j} \kappa' n_i \dot{r}'_j \partial_i \partial_j G + \sum_{i,j,k} n_i n'_j \dot{r}'_k \partial_i \partial_j \partial_k G \\
 &= \kappa' \left[(n\hat{d})(\dot{r}'\hat{d})G^{[2]} + (nr')\frac{1}{d}G^{[1]} \right] \\
 &\quad + (n\hat{d})(n'\hat{d})(\dot{r}'\hat{d})G^{[3]} + \frac{1}{d}[(nn')(\dot{r}'\hat{d}) + (nr')(n'\hat{d})]G^{[2]} \tag{B.3}
 \end{aligned}$$

and, defining $\tilde{d} = \kappa'n - \kappa n'$, we get

$$\begin{aligned}
 C_2 &= -\kappa\kappa' \dot{r}'_i \dot{r}'_j \partial_{ij} G + \tilde{d}_i \dot{r}'_j \dot{r}'_k \partial_{ijk} G + n_i n'_j \dot{r}'_k \partial_{ijkl} G \\
 &= -\kappa\kappa' \left[(\dot{r}'\hat{d})(\dot{r}'\hat{d})G^{[2]} + (\dot{r}'\dot{r}')\frac{1}{d}G^{[1]} \right] \\
 &\quad + (\tilde{d}\hat{d})(\dot{r}'\hat{d})(\dot{r}'\hat{d})G^{[3]} \\
 &\quad + [(\tilde{d}\dot{r}')(\dot{r}'\hat{d}) + (\tilde{d}\dot{r}')(\dot{r}'\hat{d}) + (\tilde{d}\hat{d})(\dot{r}'\dot{r}')] \frac{1}{d}G^{[2]} \\
 &\quad + (n\hat{d})(n'\hat{d})(\dot{r}'\hat{d})(\dot{r}'\hat{d})G^{[4]} \\
 &\quad + [(n\hat{d})(n'\hat{d})(\dot{r}'\dot{r}') + (n\hat{d})(\dot{r}'\hat{d})(\dot{r}'n')] \\
 &\quad + (n'\hat{d})(\dot{r}'\hat{d})(nr') + (\dot{r}'\hat{d})(\dot{r}'\hat{d})(nn')] \frac{1}{d}G^{[3]} \\
 &\quad + [(nn')(\dot{r}'\dot{r}') + (nr')(\dot{r}'n')] \frac{1}{d^2}G^{[2]}. \tag{B.4}
 \end{aligned}$$

For the case where the curve is a circle, equations (B.2)–(B.4) can be much simplified. Denoting $\alpha = \frac{1}{2}\kappa(t - t')$ as in section 3, the following identities hold:

$$\begin{aligned}
 \kappa &= \kappa', & d &= \frac{2}{\kappa} \sin \alpha, & \tilde{d} &= -2\kappa \sin \alpha \hat{d} \\
 \hat{d} \cdot \dot{r}' &= \hat{d} \cdot \dot{r}' = \cos(\alpha), & \hat{d} \cdot n &= -\hat{d} \cdot n' = -\sin(\alpha) \\
 n \cdot n' &= \dot{r}' \cdot \dot{r}' = \cos(2\alpha), & \dot{r}' \cdot n' &= -\dot{r}' \cdot n = \sin(2\alpha).
 \end{aligned}$$

Substituting these in (B.2)–(B.4), and expressing the trigonometric coefficients in terms of $c \equiv \cos \alpha$, the correlations become

$$\begin{aligned}
 C_0 &= (1 - c^2)G^{[2]} + (1 - 2c^2)G^{[1]}\frac{1}{d} \\
 C_1 &= (c^3 - c)G^{[3]} + (6c^3 - 5c)G^{[2]}\frac{1}{d} + (4c^3 - 4c)G^{[1]}\frac{1}{d^2} \\
 C_2 &= (c^4 - c^2)G^{[4]} + (12c^4 - 12c^2 + 1)G^{[3]}\frac{1}{d} \\
 &\quad + (28c^4 - 32c^2 + 5)G^{[2]}\frac{1}{d^2} + (8c^4 - 12c^2 + 4)G^{[1]}\frac{1}{d^3}, \tag{B.5}
 \end{aligned}$$

or, in terms of the actual derivatives $G^{(n)}$:

$$\begin{aligned}
 C_0 &= (1 - c^2)G'' + (-c^2)G'\frac{1}{d} \\
 C_1 &= (c^3 - c)G^{(3)} + (3c^3 - 2c)G''\frac{1}{d} + (c^3 - 2c)G'\frac{1}{d^2} \\
 C_2 &= (c^4 - c^2)G^{(4)} + (6c^4 - 6c^2 + 1)G^{(3)}\frac{1}{d} + (7c^4 - 11c^2 + 2)G''\frac{1}{d^2} + (c^4 - c^2 + 2)G'\frac{1}{d^3}
 \end{aligned}$$

which is equivalent to (31a)–(31c).

Appendix C. Using asymptotic series to expand the integral transforms

In section 3.2 and other sections, we discuss the number variance and form factor of some distributions. These statistics can be expressed as an integral involving the normalized correlation ((26) and (29)), for which we have an explicit expression. The expression for the correlation function (e.g. (21) or (34)) is usually very complicated, which makes the resulting integral hard to solve directly. However, given the asymptotic expansion of the normalized correlation, we can calculate the asymptotic expansion of the integral up to a small number of constants, which can be calculated numerically. The outline of this method is described here.

When calculating the number variance for large L , we encounter integrals of the form

$$I_f(L) = \int_0^L f(x) dx, \tag{C.1}$$

where $f(x) = x^k \mathcal{R}(x)$, and $\mathcal{R}(x)$ is the normalized correlation, for which the asymptotic expansion is known. We split the asymptotic expansion of f into two parts

$$f(x) \sim \sum_{n=1}^{n_0} a_n(x) + \sum_{n=n_0+1}^{\infty} a_n(x),$$

where n_0 is the number of terms a_n such that $\int_L^\infty a_n(x) dx$ diverges for every finite L (n_0 may be 0, but we will assume it is finite). We will also assume that for $n > n_0$ the integrals converge uniformly with some finite lower bound L_0).

Defining

$$D(x) \equiv \sum_{n=1}^{n_0} a_n(x), \quad C(x) \equiv f(x) - D(x), \tag{C.2}$$

we find that $C(x)$ generates an integral with known asymptotic expansion

$$\int_L^\infty C(x) dx \sim \sum_{n=n_0+1}^{\infty} \int_L^\infty a_n(x) dx \equiv - \sum_{n=n_0+1}^{\infty} b_n(L). \tag{C.3}$$

We now wish to add and subtract D from the integrand of (C.1). However, the interval $[0, L]$ might contain points which would cause the integral of D to diverge. For such cases, we split the interval at some point x_0 , which is larger than these problematic points, and do the subtraction only in the second half $[x_0, L]$. We will assume that x_0 and L are both larger than L_0 . In practice, for the functions used in this paper, there is either no points of divergence (and x_0 is chosen to be 0), or a single point of divergence at 0, in which case we choose $x_0 = 1$ (which happens to simplify the resulting expression). Using (C.2), the integral becomes

$$I_f(L) = \int_0^{x_0} f(x) dx + \int_{x_0}^L C(x) dx + \int_{x_0}^L D(x) dx.$$

The third term in this expression consists of the ‘diverging’ terms of f ; however, the integral here is finite and its asymptotic expansion is easily obtained from (C.2)

$$\int_{x_0}^L D(x) dx \sim \sum_{n=1}^{n_0} \int_{x_0}^L a_n(x) dx \equiv \sum_{n=1}^{n_0} b_n(L). \tag{C.4}$$

To handle the remaining terms, we add and subtract (C.3)

$$I_f(L) = \int_0^{x_0} f(x) dx + \int_{x_0}^\infty C(x) dx + \int_{x_0}^L D(x) dx - \int_L^\infty C(x) dx.$$

In this expression, the first two terms are having finite values independent of L , and the last two have known asymptotic expansion. Using (C.3) and (C.4), we get the final result:

$$I_f(L) \sim \mathcal{M}_f + \sum_{n=1}^{\infty} b_n(L), \quad (\text{C.5})$$

where

$$\mathcal{M}_f \equiv \int_0^{x_0} f(x)dx + \int_{x_0}^{\infty} [f(x) - D(x)]dx.$$

References

- [1] Johansson K 2002 Non-intersecting paths, random tilings and random matrices *Probab. Theory Relat. Fields* **123** 225–80
- [2] Stauffer D and Aharony A 1999 Density profile of the incipient infinite percolation cluster *Int. J. Mod. Phys. C* **10** 935–40
- [3] Stauffer D, Aharony A and Mandelbrot B B 1993 Self-similarity and covered neighborhoods of fractals: a random walk test *Physica A* **196** 1–5
- [4] Blum G, Gnuzmann S and Smilansky U 2002 Nodal domains statistics: a criterion for quantum chaos *Phys. Rev. Lett.* **88** 114101
- [5] Bogomolny E and Schmit C 2002 Percolation model for nodal domains of chaotic wave functions *Phys. Rev. Lett.* **88** 114102–+
- [6] Longuet-Higgins M S 1957 The statistical analysis of a random, moving surface *Phil. Trans. R. Soc. A* **249** 321–87
- [7] Berry M V and Dennis M R 2000 Phase singularities in isotropic random waves *Proc. R. Soc. A* **456** 2059–79
- [8] Rice S O 1945 Mathematical analysis of random noise-conclusion *Bell Syst. Tech. J.* **24** 46–156
- [9] Baik J and Rains E 2001 Symmetrized random permutations *Random Matrix Models and Their Applications (Mathematical Sciences Research Institute Publications vol 40)* ed P Bleher and A Its (Cambridge: Cambridge University Press) pp 1–19
- [10] Berry M V 1977 Regular and irregular semiclassical wave functions *J. Phys. A: Math. Gen.* **10** 2083–91
- [11] Berry M V 2002 Statistics of nodal lines and points in chaotic quantum billiards: perimeter corrections, fluctuations, curvature *J. Phys. A: Math. Gen.* **35** 3025–38
- [12] Wheeler C T 2005 Curved boundary corrections to nodal line statistics in chaotic billiards *J. Phys. A: Math. Gen.* **38** 1491–504
- [13] Urbina J D and Richter K 2004 Semiclassical construction of random wave functions for confined systems *Phys. Rev. E* **70** 015201
- [14] Foltin G, Gnuzmann S and Smilansky U 2004 The morphology of nodal lines random waves versus percolation *J. Phys. A: Math. Gen.* **37** 11363–71
- [15] Uhlenbeck K 1976 Generic properties of eigenfunctions *Am. J. Math.* **98** 1059–78
- [16] Monastra A G, Smilansky U and Gnuzmann S 2003 Avoided intersections of nodal lines *J. Phys. A: Math. Gen.* **36** 1845–53
- [17] Rice S O 1944 Mathematical analysis of random noise *Bell Syst. Tech. J.* **23** 282–332
- [18] Bogomolny E, Bohigas O and Leboeuf P 1996 Quantum chaotic dynamics and random polynomials *J. Stat. Phys.* **85** 639–79
- [19] Bogomolny E, Dubertrand R and Schmit C 2007 SLE description of the nodal lines of random wavefunctions *J. Phys. A: Math. Theor.* **40** 381–95
- [20] Mehta M L 1991 *Random Matrices* 2nd edn (Boston, MA: Academic)
- [21] Bogomolny E B, Gerland U and Schmit C 1999 Models of intermediate spectral statistics *Phys. Rev. E* **59** R1315–R1318
- [22] Kac M 1959 *Probability and Related Topics in Physical Sciences (Lectures in Applied Mathematics vol 1)* (London: Interscience)
- [23] Bohigas O 1989 Random matrix theories and chaotic dynamics *Chaos et Physique Quantique* ed M J Giannoni, A Voros and J Zinn-Justin number LII in Les Houches (Amsterdam: North-Holland) pp 87–199